# The onset of heterogeneity in the pinch-off of suspension drops.

Virgile Thiévenaz<sup>a</sup> and Alban Sauret<sup>a</sup>

<sup>a</sup> Department of Mechanical Engineering, University of California, Santa Barbara, California 93106, USA

This manuscript was compiled on February 10, 2022

12

13

14

15

16

17

20

21

11

16

At large scales, particulate suspensions flow like homogeneous viscous liquids, but at the particle scale the role of the local heterogeneity brought by the particles cannot be neglected. The volume fraction also matters: in dense suspensions, particulate effects can be felt across distances much larger than the particle diameter. Therefore, whether a suspension should behave as a homogeneous or a heterogeneous fluid is a matter of scale. Here, we consider the canonical situation of the pinch-off of suspension drops to study the behavior of suspensions at different scales. Initially, the filament of suspension thins down like a homogeneous liquid until reaching a critical thickness at which the thinning accelerates. Eventually, a region devoid of particles appears, and the break-up occurs similarly to a homogeneous viscous liquid. Although this problem have been studied for almost twenty years, the role of heterogenety in the acceleration of the pinch-off is still not understood. We show that the onset of heterogeneity corresponds to the dislocation of the suspensions where local fluctuations in particle concentration increase. We derive scaling laws for the dynamics in the heterogeneous regime and develop a model to predict the coherence length at which the discrete nature of the particles appears and demonstrate that this length depends both on the particle size and the volume fraction of the suspension. We extend this approach to polydisperse suspensions. Our work sheds light on the mesoscopic scale below which starts the heterogeneous regime and a continuum approach is not valid anymore.

Pinch-off | Suspensions | Interface | Singularity | Heterogeneity

C uspensions are ambivalent fluids. Depending on the length scale at which they flow, they can be considered homogeneous or heterogeneous. At length scales much larger than the particle size, a suspension behaves like an effective viscous liquid whose viscosity  $\eta(\phi)$  increases with the volume fraction of particles  $\phi$  (1?). However, below a certain length scale, fluctuations of particle concentration can strongly influence the flow, and the heterogeneous nature of the particles plays a crucial role. This change of scale naturally occurs during the breaking of a liquid into droplets: as a drop detaches from a nozzle, the neck that binds the drop to the nozzle thins down and eventually vanishes (2-4). In the capillary regime, the thickness of this liquid neck h(t) may undergo different self-similar regimes (5): if the flow is capillary-inertial,  $h(t) \sim (\gamma/\rho)^{1/3} (t_{\rm c}-t)^{2/3}$ , if the flow is capillary-viscous,  $h(t) \sim \gamma (t_{\rm c} - t)/\eta.$  The neck finally breaks up in a finite-time singularity at time  $t_c$ .

In practical applications, the atomized fluids can be suspensions, containing dispersed particles. For example, in ink-jet printing (6, 7), bio-fluids printing (8), and spray painting, the fluids contain solid objects, that may be rigid (pigments) or not (cells), as well as polymers and other solutes. Therefore, as a liquid neck of such complex fluids thins down, its thickness successively goes through the length scales of each component. This reveals the heterogeneous nature of the fluid: the afore-

mentioned self-similar regimes disappear and make way for thinning regimes that are specific of the components. A well-known example is the thinning of a thread of dilute polymer solution (9): initially, the liquid neck thins down like an inviscid Newtonian fluid, following the power law  $h(t) \propto (t_c - t)^{2/3}$ . At a certain point, the polymer starts interacting with the flow and the thickness h(t) decreases exponentially with time. Adding solid particles to the polymer solution does not result in a new thinning regime, but it significantly changes the threshold from one regime to another (10).

27

31

32

33

34

35

36

37

38

39

40

41

42

45

46

47

50

51

52

53

54

55

Understandably, the complexity of the problem drastically increases with the number of components, because it implies an increase of the number of length scales. Also, each kind of component (particles, polymers, cells, etc...) may exist in a range of sizes. To allow for a physical insight, we must narrow the focus to a single kind of component. Therefore, in order to isolate the viscous effects in the pinch-off of complex fluid drops, we investigate non-Brownian, neutrally-buoyant particles dispersed in a viscous liquid.

The seminal work of Furbank and Morris on the pinch-off of suspension drops revealed a two-step mechanism (11). The particles are initially homogeneously distributed in the neck. Then, when the neck has thinned down to a few particle diameters, the particle volume fraction  $\phi$  fluctuates. It was later shown that the homogeneous regime is similar to the thinning of a viscous liquid of matching viscosity (12, 13). At some point, the velocity profile in the neck becomes discontinuous (14), and the thinning accelerates (15). This transition from the homogeneous regime to the heterogeneous regime during the generation of suspension drops occurs at a critical thickness that increases with the particle diameter d, but which is not necessarily of the same order of magnitude (12). After some time, the neck becomes thinner than the particle diameter

# **Significance Statement**

The pinch-off of a liquid drop extruded from a nozzle is a canonical situation that involves a series of self-similar regimes ending in a finite-time singularity. This configuration allows exploring capillary flows over a large range of scales. In the case of suspension drops, the presence of particles breaks the self-similarity by introducing a new length scale that can be much larger than the particle diameter. This length scale is a signature of the heterogeneities and delimitates a regime in which a continuum approach of a suspension can be used from a regime where the discrete nature of the particles is involved.

V.T. and A.S. designed research; V.T. performed research; V.T., and A.S. analyzed data; and V.T., and A.S. wrote the paper.y.

The authors declare no conflict of interest.

<sup>&</sup>lt;sup>2</sup>To whom correspondence should be addressed. E-mail: asauret@ucsb.edu

ter and reduces to the interstitial liquid (16). For bidisperse suspensions, the transition depends on the relative fraction of each size of particles: the more large particles there are, the earlier the heterogeneous regime (17).

Past studies have suggested that the heterogeneous regime observed may be due to shear-thickening (18, 19), or to jamming in the neck (20). However, these explanations are incompatible with the dilute and semi-dilute cases, in which even one single particle is sufficient to trigger the acceleration of the pinch-off (14). It was reported that concentration fluctuations were amplified by the curvature gradient at the neck (21). Unfortunately, capillary effects alone cannot explain why the heterogeneous regime starts at thicknesses much larger than the particle diameter (12, 22). Accordingly, the present study aims to unify the different descriptions of suspension drop pinch-off and to clarify the role of solid heterogeneities on drop formation.

The transition to a heterogeneous regime where the particles impact the dynamics beyond a simple increase in viscosity is not specific to the pinch-off of suspension drop. Such behavior has also been reported for other flows of suspensions, dipcoating (23, 24), inclined plane (22), drop impact and sheet spreading (25), jet of suspensions (26), or spreading of a contact line (27). In all of these situations, the suspensions are found to behave either like homogeneous viscous liquids or like a heterogeneous media. The passage from one regime to another occurs at a specific length scale, which can be much larger than the particle diameter d and depends on the volume fraction  $\phi$  and d. In the discussion, we use the results of the pinch-off dynamics to conceptualize the onset of heterogeneity in free surface flows of suspensions.

We study the pinch-off of drops of suspensions, first monodisperse, then polydisperse. By considering the stability of a concentration fluctuation at the neck, we identify a new specific thinning regime, that we call the dislocation of the suspension. We derive scaling laws that describe this accelerated regime and its duration; these scaling laws match experiments conducted with a wide range of particle diameters, volume fractions up to  $\phi=50\%$ , and are applicable to monodisperse and polydisperse suspensions. Moreover, applying this approach to results from the literature (13, 18, 19, 28) enables a global vision of the pinch-off mechanisms of drops of non-Brownian suspensions.

## Thinning Dynamics

Figures 1(a)-(f) show examples of the pinch-off of drops with the pure silicone oil, further used as interstitial liquid, and suspensions of particles of diameter  $d=140\mu\mathrm{m}$  and increasing volume fractions  $\phi=2\%$ ,  $\phi=20\%$ , and  $\phi=50\%$ . The influence of the diameter of the particles composing the suspension is also illustrated for a volume fraction of  $\phi=50\%$  and particles of diameters  $20\mu\mathrm{m}$  and  $250\mu\mathrm{m}$  particles, respectively. In the absence of particles, i.e., for the interstitial fluid only, the pinch-off dynamics illustrated in figure 1(a) shows that the neck that binds the drop to the nozzle thins down as gravity and capillary pressure pull on it, and stretches into a long filament. Eventually, the thinning accelerates in the region where this filament connects to the nozzle leading to the break-up of the filament.

The initial thinning dynamics of the particulate suspensions is similar to the pure Newtonian liquid, although the dynamics is much slower due to the increase in viscosity induced by the presence of particles. In the dilute regime,  $\phi = 2\%$  shown in figure 1(b), the neck stretches into a slender filament, similarly to the pure liquid case, but this filament is eventually disturbed by the particles. Each particle trapped in the filament leads to the formation of a satellite drop, typically when the thickness of the filament is comparable to the particle size. The satellite drops are separated by viscous filaments that thin down with an associated dynamics similar to the pure liquid case. At moderate volume fraction, e.g.,  $\phi = 20\%$  illustrated in figure 1(c), the particles begin to slightly deform the liquid-air interface before they are pulled apart. Eventually, a thin filament free of particles connects the drop to the rest of the liquid at the nozzle. The resulting long filament of interstitial liquid is much thinner than the particle size and free of particles.

For dense suspensions, here  $\phi = 50\%$  in figure 1(d)-(f), the neck breaks faster, and the pinch-off dynamics depends on the particle diameter. For the  $20\,\mu\mathrm{m}$  particles, illustrated in figure 1(e), the neck stretches significantly, but its shape is very different from the pure liquid case. The thinning dynamics with large particles is highly accelerated, as illustrated with the  $250 \,\mu\mathrm{m}$  particles shown in figure 1(f). In all three dense cases shown here, the penultimate picture reveals a very short time during which the neck is made of interstitial liquid only. However, the length of this filament without particles is much shorter than the one observed for smaller volume fractions. Another significant difference during the pinch-off dynamics is the location where the break-up occurs. Indeed, the viscous liquid always breaks up near the nozzle at the top of the filament, whereas all suspensions break further away from the nozzle, especially for small particles. Besides, the thinning of suspensions is a localized phenomenon as shown by image crosscorrelation that enables to estimate the distance over which the velocity profile evolves (see Supplementary Information (29)). We find the velocity gradient to be negligible outside the volume  $h^3$  around the neck (14).

At each time step, we extract the thickness of the neck at the thinnest point h [see figure 1(a)]. The pinch-off of the neck occurs at a finite-time  $t=t_{\rm c}$ , and we thus consider the time to pinch-off,  $t_{\rm c}-t$ . Figure 2(a) reports the thinning dynamics  $h(t)=f(t_{\rm c}-t)$  of suspensions of 140  $\mu$ m particles of volume fractions  $\phi$  ranging from 2% (purple) to 50% (yellow), in real-time in figure 2(a) and in rescaled time in figure 2(b). In all plots, the time elapses from right to left. For comparison, we reported in black the thinning dynamics of the pure liquid without particles.

For the most dilute suspensions ( $\phi=2\%$ , in purple), the dynamic is barely distinguishable from that of the pure liquid. The difference appears as soon as the volume fraction is larger than 10% where the thinning dynamics observed is slower. More generally, the larger the volume fraction  $\phi$  of the suspension, the longer the thinning and the later the pinch-off. However, the shape of the thinning dynamics also changes with the volume fraction. For the most concentrated suspensions used here ( $\phi=50\%$ , in yellow), the dynamics is slower but continuously accelerated. Thus, the thinning of the suspension is not simply faster but intrinsically different and driven by a different physical mechanism.

Bonnoit *et al.* have shown that down to a certain neck thickness, a particulate suspension behaves like a homogeneous

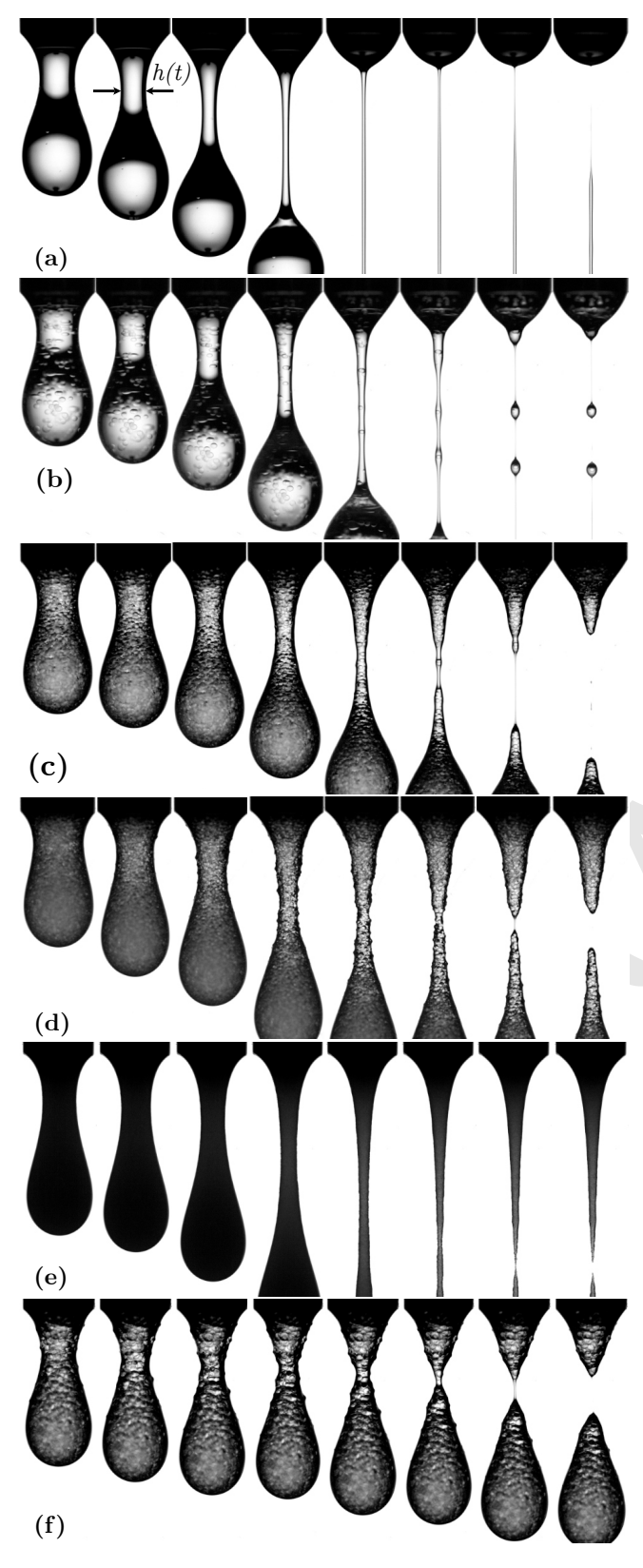


**Fig. 1.** Time series of the pinch-off of drops of (a) interstitial liquid (silicone oil, no particles), (b)  $\phi=2\%$ , (c)  $\phi=20\%$ , and (d)  $\phi=50\%$  of  $d=140\mu\mathrm{m}$  particles, (e)  $\phi=50\%$  of  $d=20\mu\mathrm{m}$  particles, and (f)  $\phi=50\%$  of  $d=250\mu\mathrm{m}$  particles. The nozzle has an outer diameter of 2.75 mm and serves as a scale bar. Videos are available in Supplementary Information (29).

liquid of matching viscosity (12). In addition, the thinning dynamics of the suspension can be rescaled onto the dynamics of another viscous liquid (17). The method consists in stretching the time to pinch-off by a factor  $\alpha_n$  and shifting it by the duration  $\Delta t$ , thus changing  $t_c - t$  to  $\alpha_{\eta}(t_c - t) + \Delta t$ . For each suspension used in this study, we compute the values of  $\alpha_n$  and  $\Delta t$  so that the early thinning dynamics of the suspension collapses onto the dynamics of the interstitial liquid. Figure 2(b) shows the rescaled thinning dynamics obtained with this method when varying the particle volume fraction  $\phi$ . Once the proper rescaling is applied, the thinning dynamics for suspensions of varying volume fraction collapse onto that of a homogeneous fluid, and the two dynamics match down to a critical thickness  $h^*$ , which depends on the particle size and the volume fraction. When the neck becomes thinner than  $h^*$ , the thinning of the suspension accelerates and becomes faster than for the equivalent liquid, as can be seen in figure 2(b).

180

181

182

183

186

187

188

189

190

192

193

194

195

196

197

198

199

200

201

202

203

204

207

209

210

211

212

214

215

216

217

218

219

221

222

223

224

225

226

227

228

229

231

232

233

234

235

236

237

The specific dynamics of the suspension when  $h < h^*$  is itself divided into two regimes, as illustrated in logarithmic scale in figure 2(c) for a suspension of volume fraction  $\phi = 40\%$ and particle size  $d = 140 \mu m$ . Below the critical thickness  $h^{\star}$ , there are two well-defined regimes, each captured by a different power-law  $h(t) \sim (t_c - t)^{\alpha}$ . The latest regime, in which h decreases linearly with time, is the viscous-capillary regime known for the pinch-off of viscous liquids (30, 31). The experiments reveal that there are no particles in the neck anymore at this time. The experimental thinning rate in this case is  $h(t)/(t_c - t) = 0.08 \,\mathrm{m.s^{-1}}$ , and the theoretical thinning rate (30) is  $0.0304 \gamma/\eta_{\rm f} = 0.066 \,\mathrm{m.s^{-1}}$  ( $\eta_{\rm f}$  denotes the viscosity of the interstitial fluid), which is slightly smaller but in good agreement with our measurement. Therefore, we can define a threshold thickness, h', below which particles do not influence the detachment of the drop anymore. The existence of the two thresholds  $h^*$  and h' leads to the definition of three regimes, shown in Figure 2(c): (I) for  $h(t) > h^*$ , an equivalent liquid regime, in which the suspension behaves like a homogeneous liquid of matching viscosity, (II) for h' < h(t) < $h^{\star}$ , a dislocation regime, during which the heterogeneity of the suspension plays a crucial role, and (III) for h(t) < h', the interstitial regime, in which the neck is devoid of particles, and the thinning is simply the thinning of the interstitial regime. Besides, the transition from (I) to (II) corresponds to a change in the evolution of the shape of the drop: for  $h > h^*$ the whole drop deforms, and for  $h < h^*$  only the neck does (see Supplementary Information (29)). The entry into the dislocation regime marks the onset of heterogeneity, where the discrete nature of the particles affects the dynamics beyond simply increasing the macroscopic viscosity.

# Onset of heterogeneity

Thinning dynamics. Deforming a dense suspension leads to the rearrangement of the particles, which causes dissipation. The local volume fraction of particles remains constant if the particles are simply sliding or rolling along each other, and fluctuates if they move away or towards each other. We hypothesize that the detachment of a suspension drop accelerates because particles start moving away from each other in the vicinity of the neck and refer to this phenomenon as the dislocation of the suspension ligament. The word dislocation is not to be taken in its meaning of defect in a lattice, for there is no order in the suspension but in its etymological meaning of

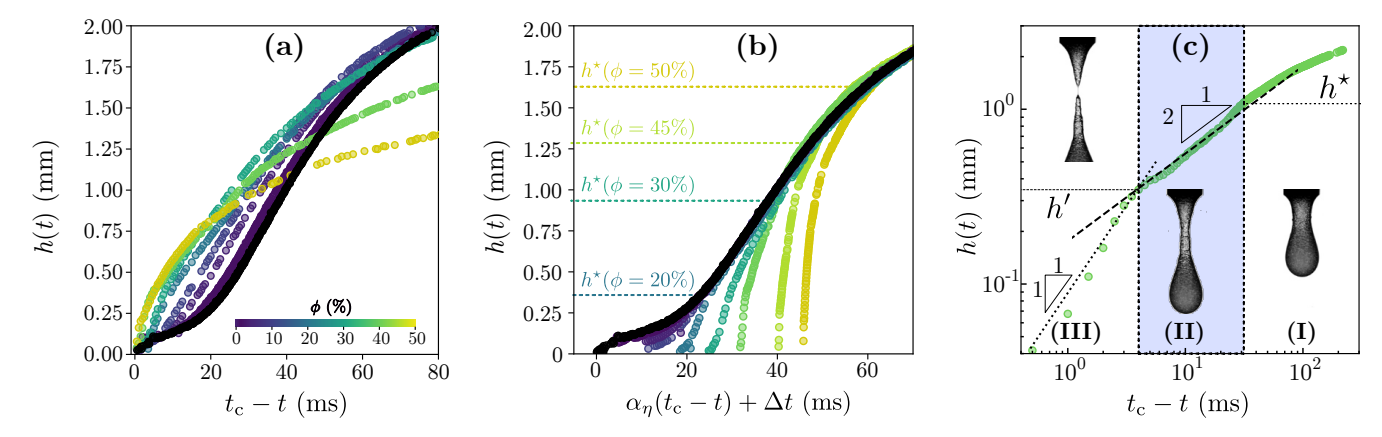


Fig. 2. (a) Thinning dynamics of suspensions of  $140\mu\mathrm{m}$  particles dispersed in silicone oil at various volume fractions  $\phi$  (colored symbols). The black symbols represent the dynamics of the interstitial fluid ( $\phi=0$ ). (b) Thinning dynamics in rescaled time. For each suspension, the time to pinch-off  $t_\mathrm{c}-t$  is shifted and stretched into  $\alpha_\eta(t_\mathrm{c}-t)+\Delta t$ , so that the dynamics overlaps with that of the interstitial fluid in the early thinning regime. The dynamics of the suspensions deviate from the interstitial liquid and accelerate at the critical thickness  $h=h^\star$ , represented by the horizontal dashed lines for volume fractions  $\phi=20,\ 30,\ 45,\ \mathrm{and}\ 50\%$ . (c) Thinning dynamics in logarithmic scale, for  $\phi=40\%$  and  $d=140\mu\mathrm{m}$ . The neck undergoes three successive thinning regimes: (I) the homogeneous liquid regime, (II) the dislocation, where  $h(t)\sim t_\mathrm{c}-t$ , similarly to a viscous liquid.

sudden separation. The dislocation mechanism begins when pulling particles apart becomes energetically favorable compared to rearranging them. In other words, dislocation is the growth of local fluctuations of the particle volume fraction.

To describe the dislocation regime, we consider a liquid film of thickness a between two portions of suspension, which represents the local fluctuation of concentration in the neck. The viscosity of the suspension is denoted  $\eta$ ; the viscosity of the interstitial liquid  $\eta_{\rm f}$ . Pulling the two portions apart at the velocity  $\dot{a}$  dissipates the power  $\eta_{\rm f} h^4 \dot{a}^2/a^3$  (see Materials and Methods). We assume that during the dislocation regime, a is of the order of magnitude of the particle diameter so that  $a \sim d$ . By balancing the power associated with the capillary forces  $\gamma h^2/(t_c-t)$  and the power associated with the viscous dissipation, we obtain the scaling law for the thinning dynamics in the dislocation regime:

$$h(t) \sim (t_{\rm c} - t)^{1/2} \sqrt{\frac{\gamma}{\eta_{\rm f}}} d$$
 [1]

Eq. [1] describes the evolution of the thickness of the neck as the capillary pressure makes particles move away from each other and captures well the dynamics in the regime (II) shown in Figure 2(c). We systematically observed this scaling law in all of our experiments for suspensions with volume fraction  $\phi \geq 20\%$ . For dilute enough suspensions, there is a range of volume fractions in which the thinning of the neck shifts directly from the equivalent regime (I) to the interstitial regime (III). Therefore, the dislocation of the suspension only occurs for concentrated enough suspensions, and the corresponding minimum volume fraction ranges from less than 2% for  $20~\mu m$  particles to 20% for  $500~\mu m$  particles.

Transitions between the different thinning regimes. Figure 3(a) reports the evolution of the critical thickness  $h^*$  at the transition between the equivalent fluid regime (I) and the dislocation regime (II) when varying the volume fraction  $\phi$  for monodisperse suspensions with different particle diameters. The thickness  $h^*$  increases both with  $\phi$  and d. Indeed, the larger the particles, the larger the thickness  $h^*$ , and the denser the suspensions, the larger  $h^*$ . Interestingly, the heterogeneities brought by the particles start occurring at a much

larger length than the particle diameter. The critical thickness of the transition between the dislocation regime (II) and the interstitial regime (III), h', depends on the particle diameter d but not significantly on the volume fraction, as illustrated in Figure 3(b). This observation is consistent with the concept of dislocation since  $h^{\star}$  marks the onset of heterogeneity when the suspension begins to dislocate, whereas h' marks the end of dislocation when the suspension in the neck is so dilute that it cannot be considered a suspension anymore.

Eq. [1] provides a prediction of the critical thickness  $h^{\star}$  as a function of the properties of the suspension. Assuming that before dislocation, the dynamics result from the balance between gravity and the effective viscosity of the suspension, the relevant time scale in the equivalent liquid regime (I) is given by  $t^{\star} = \eta/(\rho g h^{\star})$ . By combining this viscous-gravitational time scale with Eq. [1], we obtain  $h^{\star}/d \sim \eta_{\rm r}^{-1/3} (\ell_{\rm c}/d)^{2/3}$ , where  $\ell_{\rm c} = \sqrt{\gamma/(\rho g)}$  is the capillary length (1.5 mm for the silicone oil used here). We estimate the relative viscosity of the suspension  $\eta_{\rm r}(\phi) = \eta(\phi)/\eta_{\rm f}$  using the Maron-Pierce correlation (32),  $\eta_{\rm r}(\phi) = (1 - \phi/\phi_{\rm c})^{-2}$ , with  $\phi_{\rm c} \simeq 57.8\%$  for the suspensions used here (17). Finally, we obtain the evolution of the critical thickness at the dislocation regime:

$$\frac{h^{\star}}{d} \sim \left(\frac{\ell_{\rm c}}{d}\right)^{2/3} \left(1 - \frac{\phi}{\phi_{\rm c}}\right)^{-2/3}.$$
 [2]

Figure 3(c) compares the rescaled dislocation threshold  $h^{\star}/d$  to the quantity  $(\ell_c/d)^{2/3}(1-\phi/\phi_c)^{-2/3}$ , which includes the two input parameters of our experiments: the particle diameter d and the volume fraction  $\phi$ . We report in this figure the experimental results for all monodisperse suspensions considered in this study. The experimental results collapse onto a master line, which matches Eq. [2] with the prefactor 0.6. The prediction only fails for very dilute suspensions of large particles, shown by the purple points at the bottom left of figure 2(c). In this case, the concept of dislocation becomes irrelevant since there is not enough particles in the neck to consider it as homogenous even during the early stage of the pinch-off. The observation that this approach fails only in this most extreme situation emphasizes the robustness of the model, despite the rough assumptions made previously.

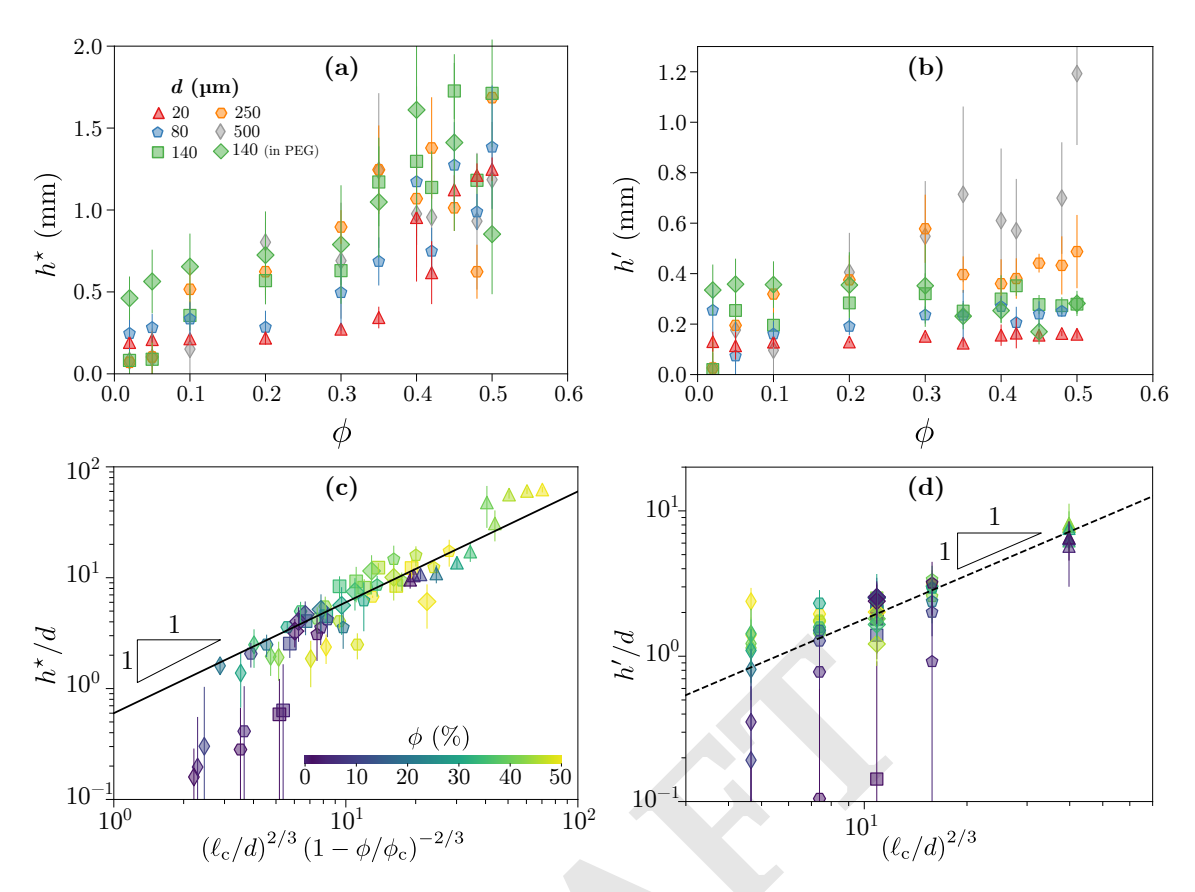


Fig. 3. (a) Critical thickness at the transition between the equivalent fluid regime (I) and the dislocation regime (II),  $h^*$ , and (b) at the transition between the dislocation regime (II) and the interstitial regime (III), h', as a function of the volume fraction  $\phi$  for monodisperse suspensions. (c)  $h^*/d$  and (d) h'/d plotted following the prediction given by Eq. [2] and Eq. [3], respectively. The different symbols represent different particle sizes, and the big diamonds represent experiments conducted with PEG. In (c) and (d), the colors represent the volume fraction, from dilute (2%, purple) to dense (50%, yellow), and the lines have a slope one.

The excellent agreement between our experiments and the model demonstrates that the acceleration of the thinning for dense enough suspensions is indeed induced by the dislocation at the neck. Changing the solvent viscosity and wetting properties, from 0.12 Pa.s (silicone oil) to 2.6 Pa.s (PEG, diamonds in figure 3(c)) does not affect the collapse of the data and the agreement between the model and the experiments. We were also able to extract the value  $h^*$  from recent experiments performed by Moon  $et\ al.\ (13)$ , which provided the thinning dynamics for suspensions of  $10\mu m$  particles. The model presented in this paper also captures their experimental data (29).

Similarly to Eq. [2], we can derive the threshold h' between the dislocation regime (II) and the interstitial regime (III). The typical time scale at this transition is given by  $t' \sim \eta_f/(\rho g h')$ . Combining this time scale with Eq. [1] yields:

$$\frac{h'}{d} \sim \left(\frac{\ell_{\rm c}}{d}\right)^{2/3}.$$
 [3]

The corresponding experimental measurements of h' plotted with respect to  $(\ell_c/d)^{2/3}$  for different monodisperse suspensions are reported in figure 3(d). Once again, we obtain an excellent agreement between the model of Eq. [3] and the experimental results. The collapse of the data onto the proposed law provides a second proof that the acceleration of the thinning is caused by the dislocation. Similar to what was observed for  $h^*$ , the prediction for h' fails for very dilute

suspensions of large particles. In these cases, it is notable that  $h^*$  and h' are very close and smaller than the particle size d. This means that the thinning switches directly from the equivalent regime to the interstitial regime. Indeed, since not enough particles are present in the neck, there is no dislocation mechanism.

341

342

343

344

345

346

348

349

350

351

352

353

355

356

357

358

359

360

361

362

363

364

Polydisperse suspensions. Monodisperse suspensions, characterized by a single length scale, the diameter d of the particles, are valuable to study due to their simplicity. Nevertheless, actual manufacturing applications or capillary processes primarily involve polydisperse suspensions. In a polydisperse suspension, each possible particle size is theoretically a relevant length scale of the flow. As a first step, we consider the dislocation of bidisperse suspensions. Bidisperse suspensions contain a volume fraction of particles  $\phi$ , split amongst  $\phi_{\rm S}$ of small particles of diameter  $d_{\rm S}$  and  $\phi_{\rm L}$  of large particles of diameter  $d_{\rm L}$ . We introduce the volume ratio of small particles  $\xi = \phi_{\rm S}/\phi$ , and the size ratio of particles  $\delta = d_{\rm L}/d_{\rm S}$  (33). For all of these suspensions and a volume fraction  $\phi$  ranging from 0 to 50%, we observe a thinning dynamic similar to that of the monodisperse case, with the three successive regimes. The main difference is that the thresholds of the dislocation regime,  $h^*$ , and h', now depend on the composition parameters,  $\xi$ , and  $\delta$ .

Polydisperse suspensions are defined by the size distribution of their particles, which we can be described through a volume-

316

317

318

319

320

322

323

324

325

326

327

330

331

332

333

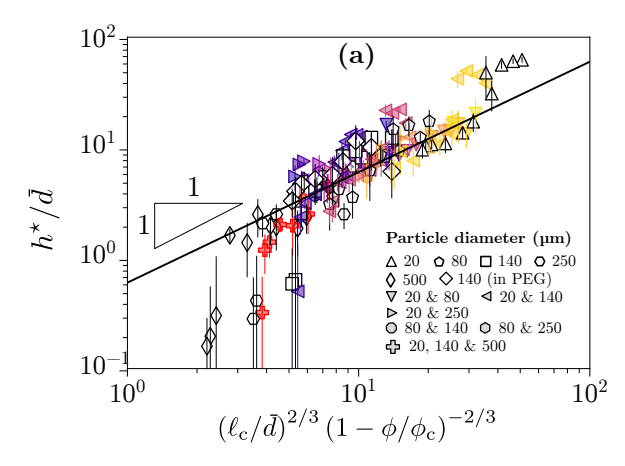
334

335

336

337

338



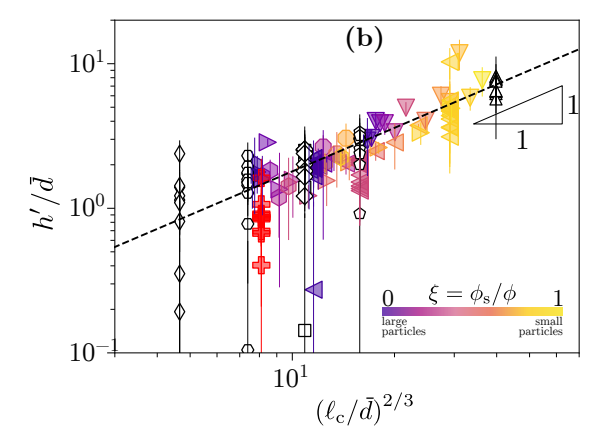


Fig. 4. (a) Critical thickness between the equivalent fluid regime (I) and the dislocation regime (II) rescaled by the volume-averaged particle diameter,  $h^*/\bar{d}$ , reported following the prediction given by Eq. [2]. (b) Critical thickness between the dislocation regime (II) and the interstitial regime (III) rescaled by the particle diameter,  $h'/\bar{d}$ , plotted following the prediction of Eq. [3]. In both figures, the black open symbols correspond to the monodisperse suspensions presented in figure 3, each symbol shape corresponding to different particle diameter. The colored symbols represent the results for the polydisperse suspensions, each symbol corresponding to a couple of particles sizes (see legend). The colors represent the share of small particles in each suspension  $\xi$  from purple for  $\xi \to 0$  (large-particle dominated regime) to yellow for  $\xi \to 1$  (small-particle dominated regime). The red crosses represent tridisperse suspensions containing one-third of  $20~\mu\text{m}$ , one-third of  $140~\mu\text{m}$  and one-third of  $500~\mu\text{m}$  particles. For all suspensions, the volume fraction varies from 2 to 50%. The experiments represented by big diamonds are conducted in PEG, and all the other experiments are performed in silicone oil.

averaged particle diameter  $\bar{d}$ . For a bidisperse suspension, this quantity is  $\bar{d} = \xi d_{\rm S} + (1 - \xi) d_{\rm L}$ . The choice of the volume-averaged diameter over the number-averaged diameter will be justified in the last section. In addition to the particle size distribution, polydisperse suspensions also differ by their lower viscosity for a given particle volume fraction than a monodisperse suspension. Indeed, the polydispersity of the particles enables a more efficient filling of the space, described by a larger value of the critical volume fraction  $\phi_c(\xi, \delta)$ . The viscosity of a polydisperse suspension can be computed from the jamming fraction of a polydisperse sphere packing, using the Maron-Pierce correlation (17, 32),  $\eta_r \sim (1 - \phi/\phi_c(\xi, \delta))^{-2}$ , where the critical volume fraction  $\phi_c$  is estimated through the model of Ouchiyama and Tanaka (34). From there, we compute  $h^*$  and h' using  $\bar{d}$  and  $\phi_c(\xi, \delta)$  in Eqs. [2]-[3].

Figure 4(a) reports the evolution of  $h^*/\bar{d}$  and figure 4(b) the evolution of  $h'/\bar{d}$ , compared to the predictions of Eqs. [2]-[3]. The colored symbols represent the bidisperse suspensions, and their color indicates the volume ratio of small particles  $\xi$ . The red crosses represent experiments performed with tridisperse suspensions composed of one-third of  $20\,\mu\mathrm{m}$ , one-third of  $140\,\mu\mathrm{m}$ , and one-third of  $500\,\mu\mathrm{m}$  particles, and a total particle volume fraction  $\phi$  ranging from 2% to 50%. The black open symbols represent the monodisperse suspensions, already shown in figures 3(c)-(d). We show all experiments on the same graph to highlight the universality of our model beyond the simplest monodisperse case usually considered in the literature.

For polydisperse suspensions, the critical thickness defining the thresholds of the dislocation regime,  $h^*$ , and h', collapse onto the same master line as the monodisperse suspensions. The limitations are the same as in the monodisperse case. More specifically, dilute suspensions of large particles do not dislocate because there are too few particles in the neck. The collapse of h' versus  $\bar{d}$  shown in figure 4(b) is even more apparent. Indeed, using a polydisperse suspension allows tuning the volume-average diameter, and these experiments clarify the dependence of h' on the particle diameter. Therefore, it appears that the dislocation regime only depends on the size

distribution through the volume-averaged diameter  $\bar{d}$  and the critical volume fraction  $\phi_c(\xi, \delta)$ .

#### Discussion

**Coherence length.** A notable feature in the pinch-off of suspension drops is that the threshold to the heterogeneous regime  $h^{\star}$  can be much larger than the diameter of the particles d and also depends on the volume fraction  $\phi$ . Indeed, a classical interpretation of the transition between a homogeneous and a heterogeneous regime is that the equivalent fluid regime stops when the scale of the flow (here the neck width h) becomes comparable to the particle size (11, 15). Such an interpretation would lead to  $h^* \sim d$ , with a proportionality factor of order one. However, our experiments demonstrate that although for dilute suspensions,  $h^*$  is indeed of the order of the particle diameter, it becomes much larger than d at larger volume fractions. For instance, for  $\phi = 50\%$ , we measure  $h^* = 1.6$ mm for 140  $\mu$ m particles, which is more than eleven times the diameter of the particles d. With 20  $\mu$ m particles, we measure  $h^{\star} = 1.24$  mm, 62 times larger than the particle diameter. More generally, Figure 3(c) shows that the ratio  $h^*/d$  varies over two orders of magnitude and strongly depends on the volume fraction. The polydisperse suspensions exhibit the same trend, as reported in Fig 4(a). Therefore, the heterogeneous structure of dense suspensions plays a role at a scale much larger than the particle diameter. A similar feature has been previously reported for the free-surface flow of dense suspensions on an inclined plane. Indeed, Bonnoit et al. (22) have defined a mesoscopic length scale that increases with the volume fraction and diverges at the critical volume transition  $\phi_c$ . The critical thickness  $h^*$  reported in this study is similar and corresponds to the limit of the homogeneous regime, at the onset of heterogeneity. In the present case, this length would also diverge when  $\phi \to \phi_c$ .

Physically, the length  $h^*$  can be seen as the coherence length of the interactions through which momentum diffuses. As a particle undergoes a fluctuation of its position, it exerts a force upon its neighbors through the lubrication film between

them. If there are contacts between particles, they transmit the momentum directly. Other forces can also act on the particles. For instance, for dilute suspension, the viscous drag on the particle should also be taken into account. If the particles are small enough, they will be subject to Brownian motion and van der Waals forces. The coherence length can then be seen as the typical length over which a fluctuation will be damped. Therefore, a stress applied on the suspension will be distributed across a volume defined by the coherence length. In the present configuration, during the detachment of the drop, the curvature of the neck generates a capillary pressure gradient between the neck and the rest of the suspension. The resulting stress will be distributed across the suspension if the neck is thicker than the coherence length. However, if the neck is thinner than the coherence length, a fraction of the suspension may experience larger local stress, which pulls the particles apart from each other and lead to the break-up through a dislocation. Therefore, here the coherence length controls the stability of the suspension against a concentration fluctuation.

443

444

445

446 447

449

450

451

452

453

456

457

458

459

460

461

462

463

464

465

466

467

468

469

470

471

472

473

474

475

476

477

478

479

482

483

484

485

486

487

488

489

490

491

492

493

494

495

497

498

499

500

501

503

Here, the words fluctuation and coherence length are meant to suggest an analogy with statistical mechanics, even if it is only a rough sketch. As the suspension flows, each particle creates a local disturbance, and one can imagine an ideal state of local equilibrium where the distance between particles is maximum so the global dissipation is minimum. Deviations from this ground state would be caused by the preparation of the suspension and by the constraints applied on the suspension (shape of the container, stress, body force). There are similarities with this approach and the Edwards ensemble (35, 36), in which the volume fraction of granular media plays the role of energy. For suspensions, volume fraction is directly linked to the rate of dissipation (by the viscosity), which is the quantity that should be minimized.

The correlation length also applies to polydisperse suspensions, although the range of sizes of the particles makes the interactions between particles more complex. Assuming that the volume of the lubrication film around a given particle is directly proportional to the volume of that particle, the lubrication pressure between small particles and between large particles is of different magnitude. This explains why  $h^*$  is relatively much larger for  $20 \,\mu\mathrm{m}$  particles than for larger particles [figure 2(c)]. Indeed, for smaller particles, the relative lubrication pressure between them is stronger, and therefore a perturbation may spread further. Therefore, the coherence length should depend not only on the number of interactions but also on the relative force of these interactions. As a result, the relevant length scale of polydisperse suspensions is the volume-averaged diameter rather than the number-average diameter. Similarly, the Ouchiyama-Tanaka model (34) with which we compute  $\phi_c$  for the polydisperse suspensions is based on a volume average of the local volume fraction. Therefore, the pinch-off dynamics, particularly the transition between the different regimes, of a polydisperse suspension can be inferred from the volume-averaged particle diameter and volume-averaged volume fraction.

Our pinch-off experiments with bidisperse suspensions reveal that they followed dynamics similar to monodisperse suspensions, meaning that pinch-off does not filter particles by size. The dislocation model enables to understand why: despite the size difference, the movement of small particle

remains strongly correlated to that of large particles, and they are not easily separated. This good agreement of our model with the bidisperse suspensions enable us to neglect self-filtration (37, 38) as a mechanism for the accelerated pinch-off.

504

505

506

507

508

509

510

511

512

513

514

515

516

517

518

519

520

521

522

523

524

525

526

527

528

529

530

531

532

533

534

535

536

537

538

539

540

541

542

543

544

545

547

548

549

550

551

552

553

554

555

556

557

558

559

560

561

**Two-particle interaction.** Contrarily to  $h^*$ , the length h' does not depend much on the volume fraction  $\phi$  [figure 3(c)]. From a neck thickness h(t) = h' and smaller, the neck reduces to a filament of interstitial liquid, without any particle in it. Just before this transition, the neck contains two particles, and the film between them experiences all of the stress acting on the neck. Thus, h' can be interpreted as the thickness that balances the viscous interaction between the last two particles of the neck and the driving force of the thinning (capillarity and the weight of the drop in the present case).

Multiple dislocations. Various studies on the pinch-off of suspension have reported qualitatively similar results. In particular, the pinch-off of suspension drops from other studies should also be explained by the mechanisms and scaling law presented in this work (18, 19). In both studies, the thinning of the suspension was empirically interpreted in terms of non-Newtonian rheology. We demonstrate in the following that the concept of dislocation can explain these results without involving a non-Newtonian rheology.

Roché et al. studied the thinning of corn-starch suspensions in water, with an average particle diameter of  $14\mu m$ (18). For  $\phi = 37\%$ , they observed a long filament that would eventually destabilize into "jammed" regions where the strain rate was zero and "flowing" regions where the thinning continues. They measured the wavelength between two flowing regions as  $700\mu m$ , although the theory of the Rayleigh-Plateau instability predicts 7 mm. Applying Eq. [2] to their configuration ( $d=14\mu\mathrm{m},\ \ell_\mathrm{c}=2.7\mathrm{mm}$  for water), we obtain  $628\mu\mathrm{m} < h^{\star} < 875\mu\mathrm{m}$  in their range of volume fraction  $(23\% < \phi < 39\%)$ . Thus, if the length of the neck is much longer than  $h^*$  when  $h(t) = h^*$ , several dislocations can happen simultaneously, and  $h^*$  is then the wavelength of the destabilization. Although the authors considered the regions not thinning as jammed, it does not necessarily need to be the case and the thinning simply continues where the viscosity is the lowest, i.e., in the dislocating regions. Pan et al. (19) studied denser suspensions of smaller particles  $(1.3 \,\mu\text{m} \le d \le 10 \,\mu\text{m})$ , with  $55\% \ge \phi \ge 59\%$ ). The thinning dynamics of their aqueous suspensions are similar to those of our viscous liquids, however they did not observe dislocation. In their configuration, the coherence length of their suspensions, calculated through Eq. [2], is a few millimeters depending on the jamming fraction. The filament is then always shorter than the wavelength of the destabilization and is therefore stable.

**Dislocation of capillary bridges.** In a recent study, Château et al. observed the pinching and break-up of capillary bridges of suspensions (28). Although their configuration is different from a pending drop, they also reported a deviation from the homogeneous liquid regime but did not provide a model to explain the variations of  $h^*$ . The scaling law for the thinning regime (Eq. [1]) matches their data for  $\phi > 20\%$ , whereas a linear law fits better for  $\phi \leq 20\%$  (29). Therefore, it seems that by plotting the last moments of the dynamics, Château et al. were observing the interstitial regime for  $\phi \leq 20\%$  and the dislocation regime for  $\phi > 20\%$ . In the latter case, the interstitial

regime may have been too short to be observed. However, their empirical scaling for  $h^*$  differs from ours, probably because the flow is different.

# Conclusion

563

564

565

569

570

571

572

573

574

577

578

579

580

581

582

583

584

585

587

590

591

592

593

594

596

597

598

600

603

604

605

606

607

608

610

611

612

613

The pinch-off of a drop of particulate suspension undergoes three regimes: first, the equivalent liquid regime, followed by a dislocation regime, and finally, the interstitial regime. In the first regime, the drop of suspension behaves like a drop of a homogeneous liquid of matching viscosity, and the particles simply rearrange when the drop deforms: this is the equivalent liquid regime. Below a certain thickness of the neck,  $h^*$ , the particles cannot simply rearrange themselves and start moving away from each other: the suspension dislocates. Finally, when particles are too far from each other to interact, the neck reduces to a filament of interstitial liquid. This is the interstitial regime, identical to the viscous-capillary regime observed during the pinch-off of a viscous liquid. This last transition occurs at the thickness h', representing the interaction range between two particles.

The dislocation of the suspension is caused by the amplification of a fluctuation of local volume fraction. We obtained in this study a scaling law for this regime,  $h(t) \sim (t_c - t)^{1/2}$ , as well as for the critical thickness  $h^*$  and h'. These predictions captured all experiments, including those performed with polydisperse suspensions. The critical length  $h^*$  translates the balance between the driving force of the interactions between the particles. This length corresponds to a coherence length of the suspension under the stress caused by capillary pressure and the weight of the falling drop.

Although our experiments considered the detachment of a drop, the concepts of coherence length and dislocation developed here go beyond this particular situation and should apply to other suspension flow. Notably, the flow of suspensions on an inclined plane exhibits a similar length scale, much larger than the particle diameters, and defines the threshold from the effective liquid regime to an intermediate regime (22). Therefore, it appears that the onset of heterogeneity in the flows of suspensions is controlled not directly by the size of the particles, but by the reach of the long-range interactions between them.

In conclusion, two length scales that depend on the particle diameter d and the volume fraction  $\phi$  characterize the capillary flow of suspension: the reach of the interactions between two particles and the coherence length of these interactions across the suspension. Since the interactions occur because of external stress, these length scales themselves depend on this applied stress. Future studies will apply these concepts to other systems involving suspensions, such as the formation of thin films (23, 24), and the fragmentation of suspension ligaments and sheets (25). In addition, beyond polydisperse suspensions, the dislocation of other kinds of complex suspensions, for example made of non-spherical particles such as fibers, or even active particles, should be considered. We expect that exploring different flows will enable a better comprehension of the interactions between particles that can lead to more predictive manufacturing processes.

### **Materials and Methods**

**Particulate suspensions.** The suspensions are made of polystyrene particles (DynoSeeds from Microbeads) with measured diameters of  $21.6 \pm 0.9 \,\mu\text{m}$ ,  $80.3 \pm 5.0 \,\mu\text{m}$ ,  $144.2 \pm 8.3 \,\mu\text{m}$ ,  $249.0 \pm 4.2 \,\mu\text{m}$ , and  $578.1 \pm 10.1 \,\mu\text{m}$ . These particles are referred in the article as  $20 \,\mu\text{m}$ ,  $80 \,\mu\text{m}$ ,  $140 \,\mu\text{m}$ ,  $250 \,\mu\text{m}$ , and  $500 \,\mu\text{m}$ , respectively. The roughness of the particles is of order 100nm (39) and their density in the range  $\rho = 1050 - 1060 \text{ kg/m}^3$ . The particles are dispersed in a densitymatched interstitial liquid to prevent buoyancy effects. We primarily use AP100 silicone oil (from Sigma Aldrich) of shear viscosity  $\eta_{\rm f} = 120$  mPa.s and surface tension  $\gamma = 24 \pm 2$  mN/m at  $20^{\circ}$ C, which perfectly wets the particle. We also conduct experiments with particles dispersed in PEG (Poly(ethylene glycol-ran-propylene glycol) monobutyl ether, Sigma Aldrich), for which  $\eta_{\rm f}=2.5~{\rm Pa.s}$ and  $\gamma = 45$  mN/m. The molar weight being as low as 3900 g/mol, this solvent can be considered Newtonian. For both interstitial liquids used in this study, the settling time of the particles is much longer than the time scale of the experiments so that the suspensions can be considered as neutrally buoyant.

621

622

623

624

626

627

628

629

631

632

633

634

635

636

637

638

639

641

642

643

644

646

647

648

649

650

651

652

653

654

655

656

657

658

660

661

662

663

665

666

667

668

670

671

673

674

675

676

677

678

679

681

682

684

685

686

687

689

690

The bidisperse suspensions are composed of the same interstitial fluid (silicone oil AP100) and made using a couple of particle sizes ( $d_{\rm S}$ ,  $d_{\rm L}$ ) chosen amongst (20  $\mu{\rm m}$ , 80  $\mu{\rm m}$ ), (20  $\mu{\rm m}$ , 140  $\mu{\rm m}$ ), (80  $\mu{\rm m}$ , 140  $\mu{\rm m}$ ), (80  $\mu{\rm m}$ , 250  $\mu{\rm m}$ ). In these experiments, we also vary the volume fraction of small particles  $\xi = \phi_{\rm S}/(\phi_{\rm S} + \phi_{\rm L})$ . The tridisperse suspensions contains one-third of 20  $\mu{\rm m}$  particles, one-third of 140  $\mu{\rm m}$ , and one-third of 500  $\mu{\rm m}$ .

**Pinch-off experiments.** The suspensions are transferred to a syringe and then manually extruded through a nozzle of outer diameter 2.75mm (for wetting liquids, the outer diameter is the relevant length scale). The extrusion is conducted slowly to avoid any inertial effects. The experiments are recorded using a high-speed camera (Phantom VEO 710) equipped with a macro lens (Nikon Micro-Nikkor 200mm AI-S). To resolve perfectly the contour of the drop and the filament, we place a LED panel (Phlox) behind the experimental setup. The time-evolution of the contour of the drop and the minimum diameter of the filament h(t) are extracted through custom-made routines using ImageJ and Python.

**Rescaling and relevant lengths.** To measure  $h^*$ , we rescale the time as  $\alpha_n(t_c-t)+\Delta t$ , and find the critical thickness at which the rescaled dynamics of the suspension deviates from the dynamics of the interstitial liquid. The stretching parameter  $\alpha_n$  accounts for the viscosity difference between the suspension and the Newtonian liquid used for comparison. The time-shift  $\Delta t$  accounts for the acceleration of the thinning due to the presence of the particles. Previous work at constant volume fraction  $\phi$  suggested that  $\alpha_n$  can be seen as the viscosity ratio between the suspension and the comparative Newtonian liquid  $\eta_{\rm r}=\eta/\eta_{\rm f}$  (17). However, the present study shows that this result does not hold if the difference in viscosity between the suspensions and the viscous liquid used for comparison is too large. Although  $\alpha_{\eta}$  follows the same divergence as the viscosity, the evolution of  $\alpha_{\eta}$  over a broad range of volume fraction  $\phi$  does not quantitatively match the viscosity of the suspensions measured with a rheometer. The length  $h^*$  is the thickness at which the rescaled dynamics of the suspension deviates from that of the interstitial fluid. We defined it systematically as the point where the thinning rate dh/dt of the suspension differs by more than 5% from that of the interstitial liquid. The length h' (smaller than  $h^{\star}$ ) is defined as the thickness at which the thinning dynamics of the filament becomes linear, i.e., follows a capillary-viscous regime.

**Dislocation.** To describe the dislocation regime, we consider the stretching of a liquid film of thickness a between two portions of suspension, pulled apart at the velocity  $\dot{a}$ . We estimate the power dissipated in the flow within. Assuming the suspension on each side of the film is much more viscous than the interstitial liquid  $(\eta_{\rm r}\gg 1)$  we approximate the flow as that of two plates pulled apart. The liquid film is then set between two cylindrical plates of diameter h, respectively, at positions z=0 and z=a. By solving the Stokes equation in the lubrication approximation, we obtain the axial velocity gradient:

$$\frac{\partial u_r}{\partial z} = 3\frac{\dot{a}}{a^3}r(2z - a).$$
 [4]

We integrate the velocity gradient over the volume of the film and obtain the order of magnitude for the power of viscous dissipation 693

694

695

696

697

698

700 701

702

703

704

705 706

707 708

709 710

711 712

713 714

715 716

722

723 724

725

726

727

728

729

730

731 732

733

734

735 736

737

738

739 740

741 742

753

754 755

756 757

760

761 762

763

764 765 772 773 774

- **ACKNOWLEDGMENTS.** This material is based upon work supported by the National Science Foundation under NSF Faculty Early Career Development (CAREER) Program Award CBET No. 1944844. We thank C. Josserand for helpful discussions.
- MM Denn, JF Morris, Rheology of non-brownian suspensions. Annu. Rev. Chem. Biomol. Eng. 5, 203–228 (2014).
- JR Castrejón-Pita, et al., Plethora of transitions during breakup of liquid filaments. Proc. Natl. Acad. Sci. 112, 4582–4587 (2015).
- A Lagarde, C Josserand, S Protière, Oscillating path between self-similarities in liquid pinchoff. Proc. Natl. Acad. Sci. 115, 12371–12376 (2018).
- JM Montanero, AM Ganán-Calvo, Dripping, jetting and tip streaming. Reports on Prog. Phys. 83, 097001 (2020).
- 5. J Eggers, E Villermaux, Physics of liquid jets. Reports on Prog. Phys. 71, 036601 (2008).
- B Derby, Inkjet printing of functional and structural materials: fluid property requirements, feature stability, and resolution. Annu. Rev. Mater. Res. 40, 395–414 (2010).
- D Lohse, Fundamental fluid dynamics challenges in inkjet printing. Annu. Rev. Fluid Mech. 54 (2022).
- SV Murphy, A Atala, 3d bioprinting of tissues and organs. Nat. Biotechnol. 32, 773–785 (2014).
- Y Amarouchene, D Bonn, J Meunier, H Kellay, Inhibition of the finite-time singularity during droplet fission of a polymeric fluid. *Phys. Rev. Lett.* 86, 3558 (2001).
- V Thiévenaz, A Sauret, Pinch-off of viscoelastic particulate suspensions. Phys. Rev. Fluids 6, L062301 (2021).
- 6, L062301 (2021).
  11. RJ Furbank, JF Morris, An experimental study of particle effects on drop formation. *Phys. Fluids* 16, 1777–1790 (2004).
- 12. C Bonnoit, T Bertrand, E Clément, A Lindner, Accelerated drop detachment in granular suspensions. *Phys. Fluids* 24, 043304 (2012).
  - JY Moon, SJ Lee, KH Ahn, SJ Lee, Filament thinning of silicone oil/poly (methyl methacrylate) suspensions under extensional flow. *Rheol. Acta* 54, 705–714 (2015).
  - MS van Deen, et al., Particles accelerate the detachment of viscous liquids. Rheol. Acta 52, 403–412 (2013).
  - RJ Furbank, JF Morris, Pendant drop thread dynamics of particle-laden liquids. Int. J. Multiph. Flow 33, 448–468 (2007).
  - A Lindner, JE Fiscina, C Wagner, Single particles accelerate final stages of capillary break-up. Europhys. Lett. 110 (2015).
  - V Thiévenaz, S Rajesh, A Sauret, Droplet detachment and pinch-off of bidisperse particulate suspensions. Soft Matter 17, 6202–6211 (2021).
  - M Roché, H Kellay, HA Stone, Heterogeneity and the role of normal stresses during the extensional thinning of non-brownian shear-thickening fluids. *Phys. Rev. Lett.* 107, 134503 (2011).
  - Z Pan, N Louvet, Y Hennequin, H Kellay, D Bonn, Drop formation in shear-thickening granular suspensions. *Phys. Rev. E* 92, 052203 (2015).
  - MZ Miskin, HM Jaeger, Droplet formation and scaling in dense suspensions. Proc. Natl. Acad. Sci. 109, 4389–4394 (2012).
  - C McIlroy, OG Harlen, Modelling capillary break-up of particulate suspensions. Phys. Fluids 26, 033101 (2014).
  - C Bonnoit, J Lanuza, A Lindner, E Clement, Mesoscopic length scale controls the rheology of dense suspensions. *Phys. Rev. Lett.* 105, 108302 (2010).
- 23. S Palma, H Lhuissier, Dip-coating with a particulate suspension. J. Fluid Mech. 869 (2019).
- 24. A Gans, et al., Dip-coating of suspensions. Soft Matter 15, 252–261 (2019).
- PS Raux, A Troger, P Jop, A Sauret, Spreading and fragmentation of particle-laden liquid sheets. *Phys. Rev. Fluids* 5, 044004 (2020).
- 747 26. J Château, H Lhuissier, Breakup of a particulate suspension jet. *Phys. Rev. Fluids* 4, 012001
  748 (2019).
- M Zhao, et al., Spreading of granular suspensions on a solid surface. Phys. Rev. Res. 2,
  022031 (2020).
- Z8. J Château, É Guazzelli, H Lhuissier, Pinch-off of a viscous suspension thread. J. Fluid Mech.
  852, 178–198 (2018).
  - 29. see supplementary material (year?).
  - J Eggers, Universal pinching of 3d axisymmetric free-surface flow. Phys. Rev. Lett. 71, 3458 (1993).
  - DT Papageorgiou, On the breakup of viscous liquid threads. Phys. Fluids 7, 1529–1544 (1995).
- É Guazzelli, O Pouliquen, Rheology of dense granular suspensions. J. Fluid Mech. 852
  (2018).
  - AP Shapiro, RF Probstein, Random packings of spheres and fluidity limits of monodisperse and bidisperse suspensions. Phys. Rev. Lett. 68, 1422 (1992).
  - N Ouchiyama, T Tanaka, Porosity of a mass of solid particles having a range of sizes. Ind. & Eng. Chem. Fundamentals 20, 66–71 (1981).
  - SF Edwards, R Oakeshott, Theory of powders. Phys. A: Stat. Mech. its Appl. 157, 1080–1090 (1989).
- 36. A Baule, F Morone, HJ Herrmann, HA Makse, Edwards statistical mechanics for jammed
  granular matter. Rev. modern physics 90, 015006 (2018).
- M Haw, Jamming, two-fluid behavior, and "self-filtration" in concentrated particulate suspensions. *Phys. review letters* 92, 185506 (2004).
- 38. SD Kulkarni, B Metzger, JF Morris, Particle-pressure-induced self-filtration in concentrated suspensions. *Phys. Rev. E* 82, 010402 (2010).

 A Deboeuf, G Gauthier, J Martin, Y Yurkovetsky, JF Morris, Particle pressure in a sheared suspension: A bridge from osmosis to granular dilatancy. *Phys. Rev. Lett.* 102, 108301 (2009).

PNAS | **February 10, 2022** | vol. XXX | no. XX | **9**